Entry Region Mass Transfer in Turbulent Pipe Flow

D. T. WASAN, W. O. JONES, and G. L. VON BEHREN

Illinois Institute of Technology, Chicago, Illinois

A general treatment is presented for mass transfer in turbulent pipe flow with special emphasis on the mass transfer entry region and the role of interfacial velocity on the rate of mass transfer. This study includes numerical solutions of the convective diffusion equation with an entering fully developed flow. Solutions for constant properties and a constant wall boundary condition are presented over a wide range of Reynolds numbers, Schmidt numbers, and aspect ratios.

An expression was developed for predicting the entry region mass transfer coefficient in both gaseous and liquid systems at ordinary fluxes with negligible interfacial velocities and at small aspect ratios. The proposed equation for a binary system is

$$N'St_{ave} = 0.24\,(N_{Re})^{-0.4}\,(N_{Sc})^{-2/3}\,(z/D)^{-0.3}$$

Experimental concentration profiles have been reported on the vaporization of acetone into a turbulent air stream within a short cylindrical test section. Data are also reported on concentration measurements in an air-carbon dioxide gaseous mixture with a large interfacial velocity at the inner surface of a porous pipe test section.

The numerical solutions of the diffusion convection equation have been compared with the experimental data in the mass transfer entry region, and a pronounced effect of the interfacial velocity on the mass transfer coefficient was found.

Most of the past experimental and analytical studies of turbulent transport have been confined to the regions of fully developed heat or mass transfer as it may occur in infinitely long transfer sections under very low flux conditions, while a limited number of studies have investigated the mass transfer entrance region. These studies have been concerned with determining the Nusselt or Stanton numbers and, to a lesser extent, the determination of the concentration profiles.

Mass transfer under low flux conditions is completely analogous to heat transfer, but the studies of this process are not as numerous as those of heat transfer. A complete literature survey on heat and mass transfer studies in both the entrance region and the fully developed region is detailed elsewhere (*7*). However, entrance region mass transfer studies with a fully developed velocity profile in a pipe will be discussed here.

Schwarz and Hoelscher (*10*) have measured the concentration profiles of water vapor in a wetted-wall column with a fully developed velocity profile at the entrance. The entering Reynolds number was 25,000 and the concentration profiles were measured at aspect ratios of 5.6, 12.4, 19.6, and 25.5.

Wasan and Wilke (*19*) and Bunch et al. (*2*) have measured mass transfer from the inner surface of a tube with the entering turbulent flow being fully developed. Both of these investigators measured the concentration profiles, Wasan's measurements being in the mass transfer entrance region of a wetted porous pipe, while the measurements of Bunch were made at only one axial position 14.2 diam. from the entrance to the wetted-wall column. The work of Wasan was accomplished at low humidities where it was experimentally observed that the velocity remained unaltered by the flux of vapor leaving the surface of the porous pipe. Cairns and Roper (*3*) have taken data at both low and high humidities; however their Reynolds number range was limited from 2,390 to 9,095, and this study is valid for simultaneous heat and mass transfer in long wetted-wall columns.

Shaw, Reiss, and Hanratty (*11*) and Son and Hanratty (*15*) have determined the entrance region mass transfer for very short aspect ratios at a Schmidt number of 2,400. By using isolated sections of the tube wall as an electrode where reduction of the ferricyanide ion occurred, Stanton numbers were reported for aspect ratios of 0.018 to 4.1 and for a Reynolds number range of 5,000 to 75,000. They (*11*) also obtained an equation for the Stanton number in the entrance region as a function of Reynolds number, Schmidt number, and aspect ratio. Several investigators have solved the energy and convective diffusion equations for binary equivolume diffusion in fully developed turbulent flow of gases in pipes. Most recently, Wasan and Wilke (*21*) attempted numerical solutions to the diffusion convection equations to establish the role of concentration level of the nondiffusing species in nonequivolume diffusion at ordinary mass transfer rates. Their results indicate that for a system at constant Schmidt and Reynolds numbers, the product of the gas-phase mass transfer coefficient and the log mean partial pressure of the nondiffusing gas is constant in the mass transfer entry region. Their results have been verified with the experimental data on absorption processes reported by Vivian and Behrmann (*17*).

THEORETICAL ANALYSIS

The physical situation considered in this section is mass transfer from the inner surface of a tube to a fluid in fully developed turbulent flow. Species A diffuses from the surface maintained at a constant vapor pressure into the inert stream. Mass transfer occurs by diffusion and bulk transport of mass by a velocity in the radial direction. In developing the diffusion convection equation, we made the following assumptions: negligible thermal diffusion, negligible pressure diffusion, no chemical reaction, constant density, steady state, a binary system, and axial symmetry. With the above assumptions the forced convection diffusion

W. O. Jones is with the Dow Chemical Company, Midland, Michigan. G. L. Von Behren is with the American Oil Company, Whiting, Indiana.

equation becomes

$$V\frac{\partial W_A}{\partial r}+U\frac{\partial W_A}{\partial z}=\frac{1}{r}\frac{\partial}{\partial r}\left[(D_{AB}+\epsilon_d)\,r\frac{\partial W_A}{\partial r}\right]+D_{AB}\frac{\partial^2 W_A}{\partial z^2}+\frac{\partial(\overline{uc})}{\partial z} \quad (1)$$

The turbulent fluctuation term $\frac{\partial(\overline{uc})}{\partial z}$ will be neglected here. By putting the above equation in dimensionless form and neglecting the last term, the convective diffusion equation to be solved is

$$-V^*\frac{\partial W^+}{\partial y^*}+U^*\frac{\partial W^+}{\partial z^+}=\frac{2}{N_{Re}(1-y^*)}\frac{\partial}{\partial y^*}\left[\left(\frac{1}{N_{Sc}}+E_d\right)(1-y^*)\frac{\partial W^+}{\partial y^*}\right]+\frac{2}{N_{Sc}N_{Re}}\frac{\partial^2 W^+}{\partial z^{+2}} \quad (2)$$

with the following boundary conditions

$$\text{IC:}\quad W_A(r,0)=0$$
$$\text{BC1:}\quad W_A(R,x)=W_{AW}$$
$$\text{BC2:}\quad \frac{\partial W_A(0,z)}{\partial r}=0 \quad (3)$$

This is the convection diffusion equation which may be solved if the mass average velocity in the axial and radial directions and the eddy diffusivity are known. The axial diffusion term has been included to determine if there is a substantial effect of axial diffusion upon the diffusion rate for short transfer section.

Considering the convective diffusion equation (2), one can obtain the solution if the various coefficients of the concentration gradient terms can be expressed as functions of radial and axial position. Expressions for the eddy diffusivity are available if the turbulent transport processes of momentum and mass transfer are assumed to be equal. Under low mass transfer rates, this assumption is a reasonable one as demonstrated by several studies published in the literature.

For the axial velocity in the core, von Karman's logarithmic velocity profile will be used, assuming it is good down to a y^+ of 20.

$$U^+=5.5+2.5\ \ln y^+ \quad (4)$$

and in the region near the wall, Wasan et al.'s velocity distribution (22, 25) will be used.

$$U^+=y^+-1.098\times10^{-4}\,y^{+4}+3.3\times10^{-6}\,y^{+6},\qquad y^+<20 \quad (5)$$

This velocity expression was derived by assuming a power series expansion of the velocity and substituting this expansion into the equations of motion.

The eddy diffusivity used in the solution of Equation (2) will be a combination of the eddy diffusivity in the wall region and an eddy diffusivity to be derived for the turbulent core. In the wall region the eddy viscosity is defined by Wasan et al. (22, 25).

$$E=\frac{\epsilon}{\nu}=\frac{4.39\times10^{-4}y^{+3}-1.65\times10^{-7}y^{+4}}{1-4.39\times10^{-4}y^{+3}-1.65\times10^{-7}y^{+4}} \quad (0<y^+<20) \quad (6)$$

The eddy viscosity in the core is derived from the linear relationship between the shear and the distance from the wall, along with von Karman's velocity distribution, giving

$$E=\frac{(1-y^*)y^+}{2.5}-1.0,\quad y^+>20 \quad (7)$$

Replacement of the radial velocity with known quantities can be accomplished by assuming that the flux of the nondiffusing species in the radial direction is zero.

$$n_B=-(D_{AB}+\epsilon)\,\rho\frac{\partial W_B}{\partial r}+W_B(\rho_A V_A+\rho_B V_B)=0 \quad (8)$$

The above estimation may be achieved by noticing that the flux of B at the wall and at the center line is zero. By assuming that the flux of B is elsewhere zero, one can equate Equation (8) to zero. Since the velocity in the radial direction can be written as

$$V=\frac{\rho_A V_A+\rho_B V_B}{\rho} \quad (9)$$

Equation (8) can be written as

$$(D_{AB}+\epsilon)\frac{\partial W_B}{\partial r}=W_B V \quad (10)$$

or in dimensionless form

$$V^*=\frac{2\left(\frac{1}{N_{Sc}}+E\right)\frac{\partial W^+}{\partial y^*}}{\left(\frac{1-W_{A0}}{W_{AW}-W_{A0}}-W^+\right)N_{Re}} \quad (11)$$

With the expressions for U^+ and E from Equations (4), (5), (6), and (7), and V^* from Equation (11), the convective diffusion equation can be put into a form for solution by finite-difference methods.

$$U^*\frac{\partial W^+}{\partial z^+}=\frac{2}{N_{Re}}\frac{1}{1-y^*}\frac{\partial}{\partial y^*}\left(\left(\frac{1}{N_{Sc}}+E\right)(1-y^*)\frac{\partial W^+}{\partial y^*}\right)+\frac{2}{N_{Re}N_{Sc}}\frac{\partial^2 W^+}{\partial z^{+2}}+\frac{2\left(\frac{1}{N_{Sc}}+E\right)}{N_{Re}\left(\frac{1-W_{A0}}{W_{AW}-W_{A0}}-W_A{}^+\right)}\left(\frac{\partial W^+}{\partial y^*}\right)^2 \quad (12)$$

NUMERICAL TECHNIQUE

Although the above equation without axial diffusion and the radial convective term has been solved by the method of separation of variables by Siegel and Sparrow (12), Kays and Leung (8), Sleicher (13), and others, the present solution will be by finite differences. A disadvantage of using the method of separation of variables is that a large number of eigenvalues are necessary to determine the entrance region behavior. Also the nonlinear term due to the radial velocity cannot be handled in a separation of variable approach.

It is difficult to obtain the solution to the above diffusion convection equation by using the classical finite-difference formulation for relatively high Reynolds numbers because the region of interest is near the wall, ($y^+ < 20$). This is the region where the concentration gradient is the steepest and thus represents the greatest resistance to mass transfer.

The difficulty of obtaining a solution can be overcome by transforming the coordinate system as suggested by Solbrig and Gidaspow (*14*). This change in the coordinate system expands the wall region and shrinks the turbulent core, thus allowing a finite-difference calculation with sufficient grid points in the region where the major resistance to mass transfer lies. By defining the new coordinate system as follows

$$dS^+ = \frac{\dfrac{dy^*}{\left(\dfrac{1}{N_{Sc}} + E\right)}}{\displaystyle\int_0^1 \frac{dy^*}{\left(\dfrac{1}{N_{Sc}} + E\right)}}$$

or

$$S^+ = \frac{\displaystyle\int_0^{y^*} \frac{dy^*}{\left(\dfrac{1}{N_{Sc}} + E\right)}}{\displaystyle\int_0^1 \frac{dy^*}{\left(\dfrac{1}{N_{Sc}} + E\right)}} \tag{13}$$

a variable grid technique is automatically put into effect. Upon substituting the new S^+ coordinate system into Equation (12), the following is obtained:

$$\frac{\partial W^+}{\partial z^+} = \frac{2\dfrac{\partial^2 W^+}{\partial S^{+2}}}{N_{Re}\,U^*\left(\dfrac{1}{N_{Sc}} + E\right)\left[\displaystyle\int_0^1 \frac{dy^+}{\dfrac{1}{N_{Sc}} + E}\right]} - \frac{2\dfrac{\partial W^+}{\partial S^+}}{N_{Re}\,U^*\,(1-y^*)\displaystyle\int_0^1 \frac{dy^*}{\dfrac{1}{N_{Sc}} + E}}$$

$$+ \frac{2\left(\dfrac{\partial W^+}{\partial S^+}\right)}{N_{Re}\,U^*\left[\displaystyle\int_0^1 \frac{dy^*}{\dfrac{1}{N_{Sc}} + E}\right]^2\left(\dfrac{1}{N_{Sc}} + E\right)\left(\dfrac{1-W_{A0}}{W_{Aw}-W_{A0}} - W^+\right)} + \frac{4\dfrac{\partial^2 W^+}{\partial z^{+2}}}{N_{Re}\,N_{Sc}\,U^*} \tag{14}$$

To determine the significance of axial diffusion for short contacting sections, Equation (14) was solved using an implicit numerical technique which is detailed elsewhere (*7*). Comparison of the results of Equation (14) with the solution of the convective diffusion equation without axial diffusion was made. Since it was found that the axial diffusion term could be neglected for most cases, Equation (14) can be simplified and the finite-difference scheme can be changed to an explicit one.

To formulate the finite-difference problem without the axial diffusion term, the Dufort and Frankel (*5*) explicit scheme was used. This finite-difference molecule retains the simplicity of a simple explicit formulation and also allows a greater range in choosing the grid size to be used.

Introducing the Dufort-Frankel molecule for the various derivatives into Equation (14), without the axial diffusion term, we obtain the basic computational equation.

$$\begin{aligned} W^+(I+1,J) &= W^+(I-1,J) + \frac{A(J)}{1+A(J)}\left(W^+(I,J+1) + W^+(I,J-1) - 2W^+(I-1,J)\right) \\ &\quad - \frac{B(J)}{1+A(J)}\left(W^+(I,J+1) - W^+(I,J-1)\right) \\ &\quad + \frac{A(J)\left(W^+(I,J+1) - W^+(I,J-1)\right)^2}{(1+A(J))\left(\dfrac{1-W_{A0}}{W_{Aw}-W_{A0}} - W^+(I,J)\right)} \end{aligned} \tag{15}$$

where

$$A(J) = \frac{4\,\Delta z^+}{N_{Re}\,U^*\,I^2\left(\dfrac{1}{N_{Sc}} + E\right)\Delta S^{+2}}$$

$$B(J) = \frac{2\,\Delta z^+}{N_{Re}\,U^*\,(1-y^*)\,I\,\Delta S^+} \tag{16}$$

and

$$I = \int_0^1 \frac{dy^*}{\dfrac{1}{N_{Sc}} + E}$$

This explicit scheme has been shown by Dufort and Frankel to always be stable under the condition that

$$O < \frac{A(J)}{I + A(J)} < 1.0 \tag{17}$$

At the center line of the tube, y^* goes to unity and hence the denominator term $(1 - y^*)$ goes to zero as does the first derivative of mass fraction in the numerator. Using L'Hospital's rule Equation (14) becomes

$$\frac{\partial W^+}{\partial z^+} = \frac{4\dfrac{\partial^2 W^+}{\partial S^{+2}}}{N_{Re}\,U^*\left(\dfrac{1}{N_{Sc}} + E\right)I^2} \tag{18}$$

at the axis of the pipe. Since the coefficient $A(J)$ is very small at the center line and presents no stability problems, the simple explicit molecule can be used.

$$W^+(I+1,J) = W^+(I,J) + 2A(J)\left(W^+(I,J-1) - W^+(I,J)\right) \tag{19}$$

Here the finite-difference solution is stable if $A(J) < 1/2$.

For the calculation of the mass transfer coefficients it is first necessary to determine the average concentration from the profiles obtained from Equation (12). The average concentration was obtained by integrating the point concentrations as follows:

$$\overline{W}^+ = \frac{\int_0^1 (1-y^*)U^* W^+ \, dy^*}{\int_0^1 (1-y^*)U^* \, dy^*} \tag{20}$$

The local Stanton number is defined as

$$N_{St} = \frac{k_g}{\overline{U}_0} \tag{21}$$

where the mass transfer coefficient is defined as assuming constant density

$$n_A = \frac{-D_{AB}\rho\left(\frac{\partial W_A}{\partial r}\right)_{r=R}}{(1-W_{Aw})} = k_g\rho\,(W_{Aw} - \overline{W}_A) \tag{22}$$

Putting the above equations into dimensionless form and combining, we obtain the following expression for the local Stanton number:

$$N_{St} = \frac{2\left(\frac{\partial W^+}{\partial y^*}\right)_{y^*=0}}{N_{Re}N_{Sc}\,(1-W_{Aw})\,(W^+{}_{Aw} - \overline{W}^+)} \tag{23}$$

This definition gives the local value of the Stanton number; however most data are reported in terms of an average Stanton number, which is defined as

$$N_{St_{ave}} = \frac{1}{L}\int_0^L N_{St}\, dz \tag{24}$$

where L is the length of the transfer section.

THEORETICAL RESULTS AT ORDINARY MASS TRANSFER RATES

To develop confidence in the numerical solution and the assumptions used, results of this solution were compared with data in the literature. First, the solution to Equation (15) was compared with the entry region mass transfer data for high Schmidt numbers. The data of Shaw, Reiss, and Hanratty (*11*), which was corrected by Son (*16*) for an error in the orifice calibration, is plotted in Figure 1 with the curves from the computer solution at the same Reynolds and Schmidt numbers. At this high Schmidt number, the major resistance to mass transfer is in the region very close to the wall, thus giving an opportunity to test the correctness of the eddy diffusivity function near the wall used in the present analysis, Equation (6). Since the agreement between the data and the computed average Stanton numbers is excellent, it will be concluded that

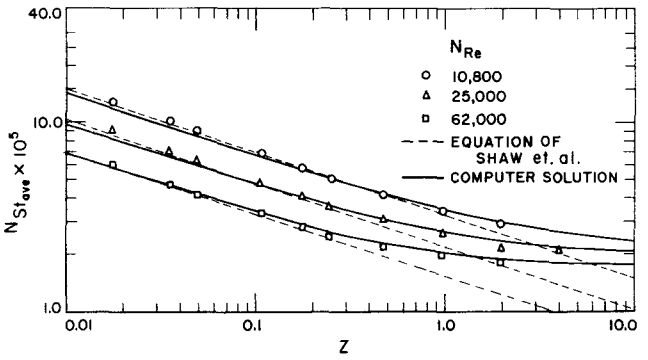

Fig. 1. Comparison of computer results with Shaw et al.'s mass transfer data corrected by Son for a Schmidt number of 2,400.

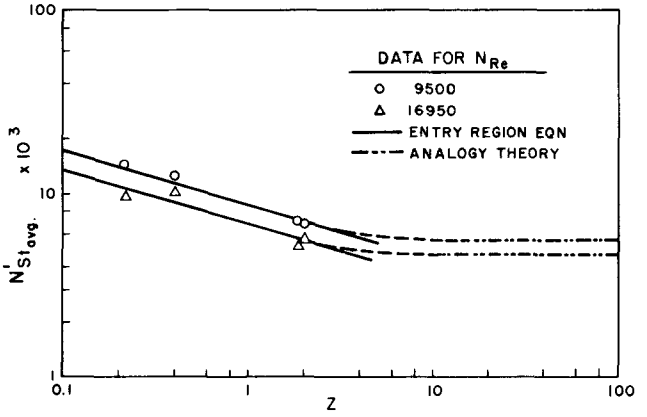

Fig. 2. Comparison of proposed entry region Equation (25) with vaporization data of Wasan and Wilke.

the eddy diffusivity function near the wall is correct and the assumption that the eddy diffusivity is equal to the eddy viscosity is reasonable. Included in Figure 1 is the entry region mass transfer equation proposed by Shaw, Reiss, and Hanratty, which agrees with the data up to an aspect ratio of 0.1, but deviates for larger aspect ratios, especially at the higher Reynolds numbers. This is not very surprising since Shaw et al. neglected the contribution of eddy diffusivity in the development of their relation.

Siegel and Sparrow (*12*) reported eigenvalues for a Prandtl number of 0.7 and the average Nusselt numbers as a function of aspect ratio for Prandtl numbers of 10.0 and 100.0. From their eigenvalues the entry region Nusselt numbers were computed and compared with the present computer solution. The results indicate that more than seven eigenvalues are necessary to predict the entry region behavior for gaseous systems. Siegel and Sparrow employed the eddy viscosity function developed by Deissler (*4*) and assumed that the ratio of eddy conductivity to eddy viscosity was unity.

A comparison was also made of the concentration profiles for the water vaporization data of Wasan and Wilke (*19*) with the computer results for two different Reynolds numbers and at three different aspect ratios in the mass transfer entry region. The flux for these data are very small; the maximum flux at the wall was 5.9×10^{-5} pounds of water vapor per square foot per second. The mass fraction profiles agreed reasonably well.

Having established some confidence in the computer calculations, we studied hypothetical cases for a Schmidt number range of 0.1 to 100,000, a Reynolds number of range of 10,000 to 100,000, and over a wide range of values of aspect ratio. These results were determined from Equation (15) for small wall mass fractions or a negligible radial component of velocity; $W_{Aw} - W_{A0}$ is of the order of 0.01 and the wall mass flux is of the order of 10^{-5} (lb.)(sq.ft.)/sec. From these results an equation for entry region mass transfer for short aspect ratios has been determined:

$$N'_{St_{ave}} = N_{St_{ave}}\, y_{BM} = 0.24\,(N_{Re})^{-0.4}\,(N_{Sc})^{-2/3}\,(z/D)^{-0.3} \tag{25}$$

It was seen from the above-mentioned computer results that Equation (25) represents the entry region mass transfer results better than Shaw et al.'s Equation (26) over the entire range of Schmidt numbers for gases and liquids. The Shaw et al. equation is of the following form:

$$N_{St_{ave}} = 0.276\,(N_{Re})^{-0.42}(N_{Sc})^{-2/3}\left(\frac{z}{D}\right)^{-1/3} \tag{26}$$

The slope of the average Stanton number versus z/D was found to vary from approximately $-1/3$ at a Reynolds number of 10,000 to less than -0.3 for a Reynolds number of 100,000. It should be pointed out that Shaw et al. (*11*) arrived at the $-1/3$ power on z/D by assuming that the eddy diffusivity is negligible compared to the molecular diffusivity. Over the range of variables investigated it was found that a power of -0.3 on the aspect ratio represents the computed entry region results satisfactorily. The Shaw et al. Equation (26) gives a slope that is too large to predict the entry region behavior for the Reynolds number range of 10,000 to 100,000.

For engineering purposes, Equation (25) may be used with the fully developed analogy results of Wasan and Wilke (*20*) to construct the local Stanton number curve. Figure 2 shows a comparison of this method to the entry region vaporization data of Wasan and Wilke (*19*). The agreement is more than satisfactory in this case. A satisfactory agreement was also obtained with Shaw's mass transfer data corrected by Son for a Schmidt number of 2,400.

EXPERIMENTAL

Apparatus and Procedure

The experimental program was initiated to obtain data on mass transfer by evaporation from the surface of a smooth porous pipe into a turbulent air stream and by injection of a gas into a turbulent air stream. By injecting air and carbon dioxide from a porous test section into a turbulent air stream, it was also possible to study the effect of the radial component of velocity upon the convective transport.

The experimental apparatus designed for this study is shown in a schematic presentation (Figure 3). Inlet room temperature air was heated by two electrical heaters before entering the blower. At the discharge outlet was a gate valve for regulating blower output to obtain the desired Reynolds number. From the blower, the air was passed through an 11-ft. diverging-converging section to reduce the turbulence caused by the blower. Eighteen inches of fiberglas filter pad were inserted in the enlarged section to further dampen blower disturbances and achieve nearly plug flow. In order to ensure a fully developed velocity profile, 30 ft. of seamless aluminum pipe, 6-in. I.D., were used as a developing section.

The test section was annular in design to allow mass transfer to occur from the surface of a porous cylinder to the air stream. The test section annulus consisted of a 6-in. I.D. aluminum cylinder used as the outer shell. Flanges with machined recesses served as end pieces to connect the test section to the developing and exit sections. A main and a swing feed tank delivered liquid to the annulus for wetting of the porous pipe wall. To maintain uniform liquid temperatures at any position, fluid was withdrawn from exit ports and run through a heat exchanger bank and was then returned through a staggered tee pipe manifold. When gaseous systems were studied, the main feed tank served as a surge tank to allow the gas to be fed to the test section under uniform pressure. Feed preheat was obtained from a steam heat exchanger located at the feed tanks.

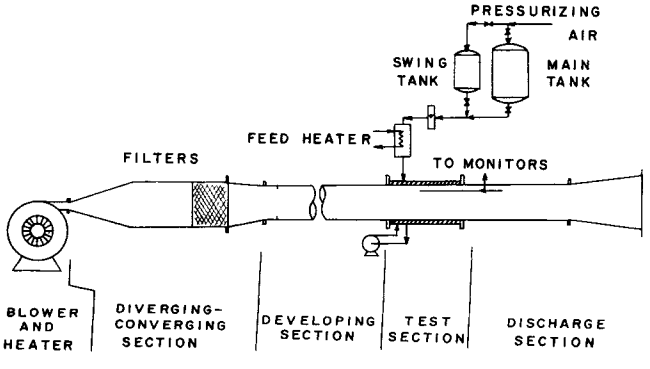

Fig. 3. Schematic drawing of experimental apparatus.

Thermocouples were placed at 30 positions throughout the porous pipe. This series of thermocouples recorded both axial and radial temperature profiles on the inside, middle, and outside surfaces of the porous pipe. Small holes were drilled into the test section at aspect ratios of 0.25, 2.0, 4.0, and 5.75 for the thermocouple wells. The thermocouples were cemented in place with Silastic 732R cement. Surface thermocouples did not actually lie on the surface but were placed as close to the surface as possible with a thin layer of Silastic covering the weld.

The exit gas mixture is exhausted to the atmosphere after passing through a conical diffuser to prevent back pressure effects.

Data points were collected from a pitot tube connected to a vertical and horizontal gear train mounted on the pipe to the rear of the test section. The tip of the impact tube was filed to an outside diameter of 0.4 mm. or 0.0025 in. The pitot tube was connected to a inclined tube micromanometer (range: 0-0.2 in. H_2O) for velocity readings. Concentration readings were taken isokinetically from the impact side of the pitot tube, using a gas chromatograph to analyze the sample. Temperatures at any point within the test section were measured using 30-gauge copper-constantan thermocouples mounted on each side and immediately to the rear of the tip of the impact side of the pitot tube.

Runs were made at Reynolds numbers between 20,000 and 64,000. Vaporization experiments were made using an acetone. For the gaseous runs air and carbon dioxide were supplied to the test section annulus. All runs were made at a wall temperature of 80°F. and at atmospheric pressure. The details of the equipment and procedure used can be found in two theses (*7, 18*).

Equipment performance was checked to verify the assumption of fully developed symmetrical flow by comparing data for the binary system with semitheoretical velocity profiles.

EXPERIMENTAL RESULTS AND DISCUSSION

Table 1 gives the conditions under which the acetone runs were made. The entering Reynolds number was calculated using the entering average velocity and the kinematic viscosity of the entering air, while the Reynolds number at the wall was based upon the same average velocity, but the kinematic viscosity was determined from the temperature and composition at the wall. The Schmidt number was also calculated at the wall conditions, and the mass fraction at the wall was calculated from the vapor pressure determined by the temperature measurements of the surface thermocouples. Table 2 gives the calculated data for the runs. The minimum flux at wall was 6.4×10^{-4} and the maximum flux was 1.9×10^{-2} pounds of acetone vapor per square foot per second. When these fluxes are compared with the recent data of Wasan and Wilke (*19, 23*), our flux levels are greater by a factor of 10 to 1,000. The difference is due to the high interfacial velocity at the wall. Therefore our experiments constitute a high flux mass transfer system hitherto unemployed.

The average mass fraction was obtained by graphical integration of the concentration profile using the following equation:

$$\overline{W}_A = \frac{2\int_0^1 U \rho W_A (1 - y^*)\, dy^*}{\overline{U}_0} \qquad (27)$$

Table 1. Operating Conditions for Acetone Vaporization and Carbon Dioxide Injection

Run	System	z/D ratio	Inlet N_{Re}	N_{Re} based on wall conditions	N_{Sc} based on wall conditions	Wall mass fraction W_{Aw}
1	Acetone-air	1.5	21,500	32,000	1.1	0.45
2		3.0				0.45
3		6.0	21,500	32,000		0.45
4	Acetone-air	1.5	45,000	69,000	1.1	0.45
5		4.0	45,500	69,000		0.46
6		6.0	44,700	69,000		0.47
7	Acetone-air	1.5	64,000	100,000	1.1	0.46
8		3.0	63,400	98,000		0.43
9		6.0	64,000	100,000		0.43
10	Carbon dioxide-air	0.5	24,000	27,000	0.88	0.23
11		2.0	23,900	27,000		0.26
12		4.0	24,300	28,300		0.28

To determine the radial velocity at the wall, we first calculated the flux at the wall from an overall balance.

$$n_{A_w} = \frac{\overline{U}_0 \rho \overline{W}_A}{4\ z/D} \tag{28}$$

Then the radial velocity was calculated from the following equation:

$$V_W = \frac{n_{A_w}}{\rho_W} \tag{29}$$

since n_B is zero at the wall. The dimensionless radial velocity is defined as

$$\phi = \frac{V_w}{U_{\tau 0}} \tag{30}$$

where $U_{\tau 0}$ is the friction velocity based upon entering conditions. Next an average Stanton number was calculated from the integrated data, assuming the density was constant. This was done to compare with the numerical results from the solution of Equation (17), which also has in it the assumption of constant density. The Stanton numbers were calculated from the following equation:

$$N_{St_{ave}} = \frac{1}{4\ z/D \left(\dfrac{W_{A_w}}{\overline{W}_A} - 1 \right)} \tag{31}$$

Figures 4 and 5 give a comparison of the experimental mass fraction profiles with the numerical solution of the convective diffusion equation neglecting axial diffusion but including the convective term in the radial direction. The radial velocity was not accounted for as in the low flux calculations, but was replaced by a dimensionless polynomial of the form:

$$\frac{V}{V_w} = 1 - 0.05\ y^* - 0.564\ (y^*)^2 - 0.386\ (y^*)^3 \tag{32}$$

It was found that accounting for the radial component of velocity, as in Equation (11), the predicted concentration profiles and the Stanton numbers were lower than the experimental data. In order to account for the observed difference, velocity data from the injection of air and carbon dioxide into the turbulent stream were used to assess the radial velocity contribution.

It was found that on a V/V_w versus y^* plot the radial velocity takes approximately the shape of a parabola, V/V_w being 1.0 at the wall and zero at the center line. The constants appearing in Equation (32) were determined by fitting the cubic equation to the curve. To apply the results from the injection experiments to the acetone data, it was necessarily assumed that the radial velocity is not a strong function of the aspect ratio but a function of V_w and therefore ϕ only. To validate this assumption, extremely precise measurements of the velocity profiles are

Table 2. Calculated Data

Run	Average mass fraction W_A	Radial flux at the wall n_{A_w} lb.$_A$/(sec.)(sq.ft.)	Radial velocity at the wall, V_w, ft./sec.	Dimensionless wall Velocity, $\frac{V_w}{U_\tau}$	Average Stanton number $N_{St_{ave}} \times 10^3$	Computed Stanton number $N_{St_{ave}} \times 10^3$
1	0.0106	0.00093	−0.01033	−0.0228	4.3	3.90
2	0.0146	0.00064	−0.0071	−0.0156	2.8	3.55
3	0.0302	0.000656	−0.0073	−0.016	3.04	3.30
4	0.00688	0.00127	−0.0149	−0.0175	2.6	3.15
5	0.0237	0.00164	−0.0182	−0.0214	3.5	2.85
6	0.0347	0.0016	−0.0178	−0.021	3.1	2.75
7	0.00715	0.0186	−0.0206	−0.018	2.14	2.82
8	0.0113	0.0147	−0.0163	−0.0142	2.7	2.60
9	0.0292	0.0190	−0.0211	−0.0183	2.81	2.5
10	0.00331	0.00106	−0.0137	−0.0274	7.16	6.2
11	0.0191	0.00076	−0.0098	−0.0196	4.6	5.0
12	0.0191	0.00076	−0.0098	−0.0197	4.3	4.6

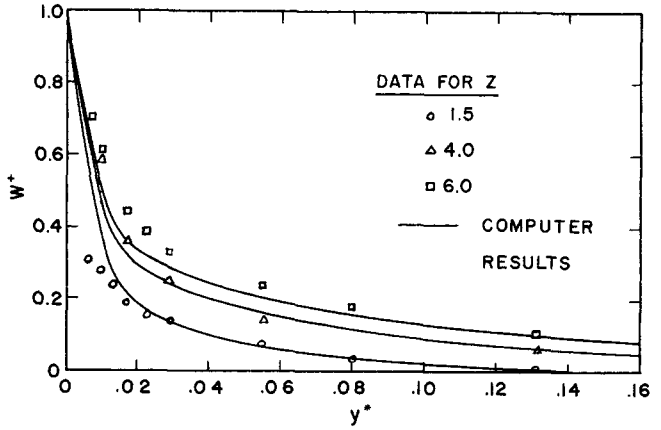

Fig. 4. Mass fraction profiles for the present acetone data at a Reynolds number of 44,700, a Schmidt number of 1.1, and a ϕ of 0.02.

necessary to reduce any quantitative information from the evaporation experiments with an $V_w/U_{\tau 0}$ ratio on the order of 0.02.

The finite-difference formulation is the same as Equation (15) except that the radial velocity was replaced as described above, and two different Reynolds numbers were used in evaluating the coefficients for the finite difference scheme. The entering Reynolds number was used to determine the friction factor and velocity distribution. However, the wall Reynolds number was used in evaluating the coefficients of Equation (15), having the effect of evaluating the physical properties at the wall. When this is done, Equation (15) becomes

$$W^+(I+1,J) = W^+(I-1,J) + \frac{A(J)}{1+A(J)}\left(W^+(I,J+1) + W^+(I,J-1) + 2W^+(I-1,J)\right) - \frac{(B(J)+VC(J))}{1+A(J)}\left(W^+(I,J+1) - W^+(I,J-1)\right) \quad (33)$$

where

$$VC(J) = \frac{\frac{V}{V_w}\phi\sqrt{\frac{f}{2}}\Delta z^+}{U^*\left(\frac{1}{N_{Sc}}+E\right) I\,\Delta S^+} \quad (34)$$

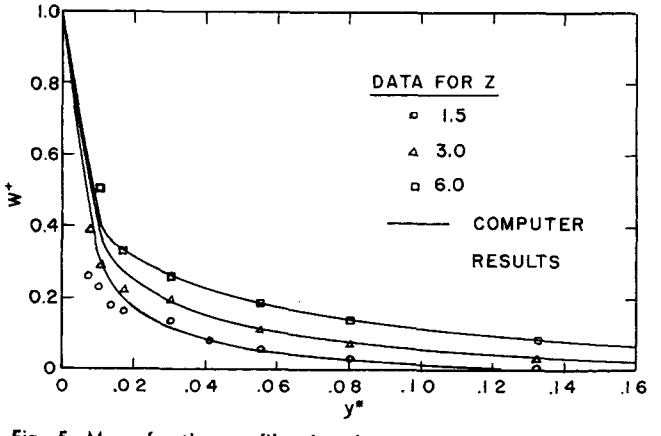

Fig. 5. Mass fraction profiles for the present acetone data at a Reynolds number of 64,000, a Schmidt number of 1.1, and a ϕ of 0.017.

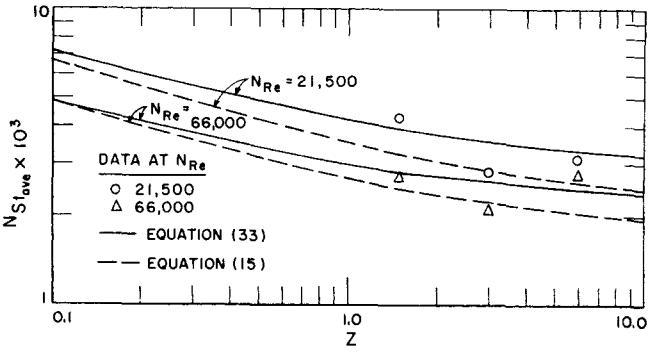

Fig. 6. Comparison of the experimental Stanton numbers for acetone with the numerical solutions at a Schmidt number of 1.1.

Here V/V_w is given by Equation (32) and ϕ is determined from the mass flux at the wall corresponding to each experimental run. The velocity profile is not significantly altered by a ϕ on the order 0.02. Therefore the velocity profile used in the finite-difference scheme is the same as for $\phi = 0$. Also the eddy diffusivity was assumed to be unchanged. As can be seen in the comparison with the experimental data the numerical solution predicts the mass fraction profiles reasonably well, except very near the wall.

In Figures 6 and 7, the experimental Stanton numbers are presented with the computer solution as a function of the aspect ratio. The numerical solution, including the radial velocity term of Equation (34), predicts the Stanton number better than if the velocity had been determined from the formulation of Equations (11) and (15). The experimental Stanton numbers lie consistently above the computer results of Equation (15), which was derived assuming n_B is zero everywhere.

The experimental data were also compared with the numerical solution of the diffusion convection equation assuming no radial convective velocity, and the calculated Stanton numbers were found to differ from experimental values by as much as 50%. Therefore it may be concluded that the radial convective velocity greatly affects the mass transfer rates.

Figure 8 shows the average Stanton numbers as calculated by Equation (33) versus the experimental Stanton numbers for the acetone vaporization and the carbon dioxide injection runs. The data variation is within 23% of the computed value, the maximum deviation was 22.8%, while the smallest difference was 2.5%.

An attempt was also made to compare the present en-

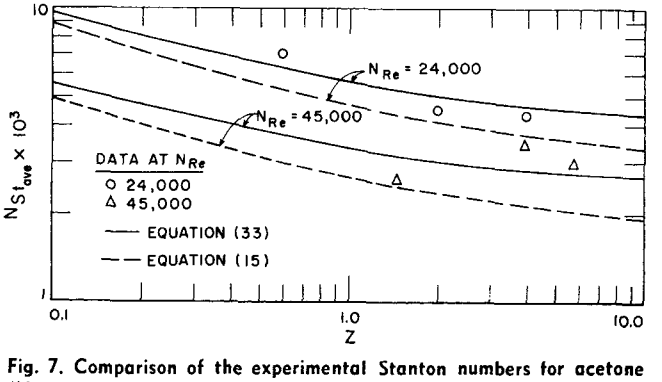

Fig. 7. Comparison of the experimental Stanton numbers for acetone (N_{Re} = 45,000) and carbon dioxide (N_{Re} = 24,000) with the numerical solutions.

trance region mass transfer results with those calculated from the well-known film theory (*1*) at these high fluxes. The film theory results were found to be higher than the present values. The difference can be attributed to the high interfacial velocities, and the film theory gives erroneous values (*24*).

The agreement between the theoretical predictions and the present experimental data for binary systems appears to be within the experimental limitations. Discrepancies between the theory and the experiment may be due to the following uncertainties: the temperature at the liquid-gas interface and hence the vapor pressure; the thickness of the liquid film; the placement of the probe near the interface; and the variation of the physical properties in the region immediately adjacent to the wall. The flow of liquid to the surface of the porous pipe was much larger than the quantity of acetone evaporated and hence the surface was continuously renewed with new liquid. Also, the temperature gradient through the porous pipe was less than 5°F., and for this reason it was felt that the surface temperature was determined with a fair amount of certainty. Probe placement was accomplished visually before each traverse by opening the test section at the forward flange and hence the position of the probe was subject to only small errors.

Finally, the assumption of a constant density introduces error. The physical and transport properties vary as a function of the radius. However, by evaluating them at the wall where the molecular properties are most important, this error has been minimized. Furthermore, as concluded by Emanual and Olander (*6*), the role of variations in density and other physical properties is not as significant as the role of the interfacial velocity in these high mass flux systems.

CONCLUSIONS

1. A computer solution has been developed which can be used to predict correctly heat and mass transfer rates for ordinary and high fluxes in the entry and fully developed regions for nonequivolume turbulent transport with constant fluid properties. The only inputs for the program necessary to predict heat or mass transfer coefficients at any aspect ratio are the axial and radial velocity, eddy diffusivity function, fluid properties, and Reynolds number.
2. The present numerical solution indicates that the contribution of axial diffusion can be neglected for turbulent transport in both gaseous and liquid systems.
3. Previous analytical solutions for entrance region heat or mass transfer are not very accurate for predicitng the Nusselt or Stanton numbers for small aspect ratios and for nonequivolume turbulent transport.
4. An equation (25) for entrance region mass transfer was developed to predict the Stanton number for small z/D ratios at ordinary mass transfer rates. Equation (25) is developed for a range of Schmidt numbers from 0.1 to 100,000 and for a range of Reynolds numbers of 10,000 to 100,000. For engineering calculation, this equation may be utilized with the fully developed analogy theory to compute the local Stanton number in a binary system.
5. Comparison of the numerical solutions with data at high fluxes for the vaporization of acetone and the injection of carbon dioxide showed that they predicted reasonably well the concentration profiles and the Stanton numbers when the radial variation of velocity in the wall region is taken into account. A significant effect of the interfacial velocity on the transfer coefficient is found. But more precise data on axial and radial velocity profiles under high flux conditions are necessary to establish more generally the role of the variation of radial velocity on mass transfer rates.

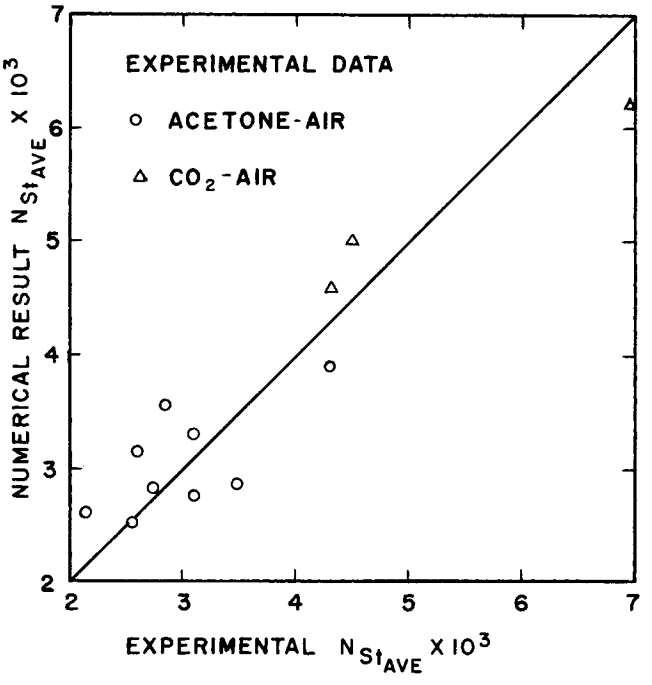

Fig. 8. Comparison of experimentally determined Stanton numbers with the computed Stanton numbers.

ACKNOWLEDGMENT

Financial support for this study was partly provided by an American Oil Company fellowship, the Institute of Gas Technology, and the National Science Foundation under Grant GK-255. The authors also thank Professor S. Leipziger for his participation at the earlier stages of this study, and the Manufacturing Department of the American Oil Company for technical assistance.

NOTATION

A, B = coefficients as defined by Equation (16)
c = fluctuation in concentration
D = diameter of the pipe
E = dimensionless $\frac{\epsilon}{\nu} = \frac{\epsilon_d}{\nu}$
f = friction factor
k_g = binary mass transfer coefficient
N_{Re} = Reynolds number $= \overline{U}_0 D/\nu$
N_{Sc} = Schmidt number $= \nu/D_{AB}$
$N_{St_{ave}}$ = average Stanton number $= k_g/\overline{U}_0$
$N'_{St_{ave}}$ = average Stanton number including y_{Bm} ($N'_{St_{ave}} = N_{St_{ave}}\, y_{Bm}$)
n_B = mass flux of B with respect to stationary coordinates
r = radial distance
R = radius of the tube
S^+ = dimensionless coordinate as defined by Equation (13)
u = fluctuating velocity in axial direction
U = time-average velocity in axial direction
U^+ = dimensionless universal velocity $= U/U_\tau$
U_τ = shear velocity $= \overline{U}_0 \sqrt{f/2}$
$\overline{U}_0$ = average velocity in axial direction
U^* = dimensionless velocity $= U/\overline{U}_0$
V^* = dimensional radial velocity as defined by Equation (11)
V = radial velocity
W^+ = dimensionless mass fraction, $\frac{W_A - W_{A0}}{W_{Aw} - W_{A0}}$

$\overline{W}^+$ = dimensionless average mass fraction
W_{Aw} = mass fraction at the wall
$\overline{W}_A$ = average mass fraction
y_{Bm} = log mean concentration of nondiffusing species, dimensionless
y = distance from the pipe wall, $R - r$, ft.
y° = dimensionless distance from the pipe wall, $1 - r/R$
y^+ = dimensionless distance from the pipe wall, $y\ U_\tau/\nu$
Z = aspect ratio = z/D
z = axial direction, axial distance
Z^+ = dimensionless axial distance = z/R
ρ = density
μ = viscosity
ν = kinematic viscosity
ϵ = eddy viscosity
τ = shear stress
ϕ = blowing factor, $V_w/U_{\tau 0}$
A = diffusing species
B = nondiffusing species
0 = incoming stream
r = radial direction
w = wall value
z = axial direction

LITERATURE CITED

1. Bird, R. B., W. E. Stewart and E. N. Lightfoot, "Transport Phenomena," pp. 658-663, Wiley, New York (1960).
2. Bunch, D. W., and M. R. Strunk, *AIChE J.*, 11, 1108 (1965).
3. Cairns, R. C., and G. H. Roper, *Chem. Eng. Sci.*, 3, 97 (1954)
4. Deissler, R. G., *NACA TN 3016* (1953).
5. Dufort, E. C., and S. P. Frankel, *Math Tables Aids Computation*, 7, 135 (1953).
6. Emanual, A., and D. R. Olander, *Intern. J. Heat Mass Transfer*, 7, 539 (1964).
7. Jones, W. O., Ph.D. thesis, Illinois Inst. Techn., Chicago (1969).
8. Kays, W. M., and E. Y. Leung, *Intern. J. Heat Mass Transfer*, 6, 537 (1963).
9. Reiss, L. P., Ph.D. thesis, Univ. Illinois, Urbana (1963).
10. Schwarz, W. H., and H. E. Hoelscher, *AIChE J.*, 2, 101 (1956).
11. Shaw, P. V., L. P. Reiss, and T. J. Hanratty, *ibid.*, 9, 362 (1963).
12. Siegel, R., and E. M. Sparrow, *Trans. ASME*, 82c, 152 (1960).
13. Sleicher, C. A., *ibid.*, 80, 693 (1958).
14. Solbrig, C. W., and Dimitri Gidaspow, *Intern. J. Heat Mass Transfer*, 11, 155 (1968).
15. Son, J. S., and T. J. Hanratty, *AIChE J.*, 13, 689 (1967).
16. Son, J. S., M.S. thesis, Univ. Illinois, Urbana (1965).
17. Vivian, J. E., and W. C. Behrmann, *AIChE J.*, 11, 656 (1965).
18. Von Behren, G. L., M.S. thesis, Illinois Inst. Technol., Chicago (1969).
19. Wasan, D. T., and C. R. Wilke, *Lawrence Rad. Lab. Rept. UCRL-16221* (Jan. 1965).
20. ———, *Intern. J. Heat Mass Transfer*, 7, 87 (1964).
21. ———, *AIChE J.*, 14, 577 (1968).
22. Wasan, D. T., C. L. Tien, and C. R. Wilke, *ibid.*, 9, 567 (1963).
23. Wasan, D. T., R. M. Davis, and C. R. Wilke, *ibid.*, 14, 227 (1968).
24. Wasan, D. T., and C. Y. Yoo, manuscript in preparation.
25. Wasan, D. T., T. K. Subramaniam, and S. S. Randhava, *Chem. Eng.*, 165 (1966).

Manuscript received September 15, 1969; revision received January 24, 1970; paper accepted January 30, 1970. Paper presented at AIChE Washington meeting.

Phase Equilibria in the Methane-Ethane-Propane-*n*-Pentane-*n*-Hexane-*n*-Decane System

JURIS VAIROGS, A. J. KLEKERS, and W. C. EDMISTER
Oklahoma State University, Stillwater, Oklahoma

An experimental facility for vapor-liquid equilibrium measurements at high pressures (100 to 15,000 lb./sq. in. abs.) and ordinary temperatures (100° to 300°F.) on multicomponent mixtures is described. The vapor-liquid phase behavior of a six-component hydrocarbon mixture, which simulated a natural gas and a condensate, was studied with this apparatus. Measurements were made at 150° and 250°F. and pressures ranging from 100 lb./sq. in. abs. to the single-phase pressures for these systems and temperatures.

Vapor-liquid equilibrium K values for the components of natural gas and condensate at high pressures are used by reservoir engineers in making condensate depletion calculations and by process engineers in designing hydrocarbon separation facilities for the gas and condensate production.

The natural gas-condensate system is a multicomponent mixture that is difficult to break down into components. Natural gas compositions can usually be characterized by the names and amounts of specific compounds (that is, hydrocarbons and related gases, such as nitrogen and carbon dioxide). Condensates, on the other hand, are usually characterized in terms of both real and hypothetical components, the latter being identified by atmospheric boiling point ranges.

In this technique of characterization, a hypothetical component contains many actual components, all in small concentration, that fall in the specific boiling point range. For the prediction of thermodynamic properties of such hypothetical components, it is necessary to use average physical properties, such as density, molecular weight, vapor pressures, and vapor-liquid K values. Approximations of this kind may be acceptable in depletion and design calculations, but should not be a part of an experimental study of vapor-liquid equilibria, as was learned in a recent thesis project (9) carried out at Oklahoma State

A. J. Klekers is with Celanese Company, Corpus Christi, Texas.
J. Vairogs is with Cities Service Oil Company, Tulsa, Oklahoma.